Journal of
Flood Risk Management

Pluvial flooding in urban areas: the role of surface drainage efficiency

A. Palla[1], M. Colli[1], A. Candela[2], G.T. Aronica[3] and L.G. Lanza[1]

1 Department of Civil, Chemical and Environmental Engineering, University of Genova, Genoa, Italy
2 Department of Hydraulic, Environmental, Aerospace and Materials Engineering, University of Palermo, Palermo, Italy
3 Department of Civil, Computer, Construction, Environmental Engineering and Applied Mathematics, University of Messina, Messina, Italy

Correspondence
Anna Palla, Department of Civil, Chemical and Environmental Engineering, University of Genova, via Montallegro 1, 16145 Genoa, Italy
Tel: +390103532301
Email: anna.palla@unige.it

DOI: 10.1111/jfr3.12246

Key words
Hazard maps; inlet efficiency; modelling; pluvial flooding; surface drainage.

Abstract

Pluvial flooding in urban areas may derive from the limited or temporarily reduced efficiency of surface drainage, even when the underlying storm sewers are properly designed. This study focuses on the impact of uncertainties in the operational condition of the surface drainage system on pluvial flood hazard. The flood propagation model FLURB-2D is implemented on a selected study area in the town of Genoa (Italy). Synthetic hyetographs based on the Chicago and bivariate copula methods with suitable return periods are used as input. While simulating the design rainfall, inlet operational conditions are varied stochastically using a Monte Carlo approach. Results confirm that microtopography has the potential to impact the efficiency of surface drainage and consequently to produce local flooding, with significant water depth in zones of flow concentration. Furthermore, the derived inundation maps allow the highlighting of areas with insufficient design of the surface drainage system (inlet size and positioning).

Introduction

Pluvial flooding occurs as a consequence of high rainfall rates when surface runoff (flowing along preferential pathways, typically roads, footpaths, natural ground depressions, small water courses, etc.) cannot be efficiently conveyed into the underground storm water drainage system (surface drainage deficiency). In other cases, the underground storm water drainage system itself overflows (drainage system failure) (Ball and Alexander, 2006; Maksimović *et al.*, 2009).

The hydraulic performance of urban drainage systems can be dramatically affected by the operational condition of its components as in the case of inlets, through which surface storm-water runoff enters the underground storm water drainage (Despotovic *et al.*, 2005; Djordjević *et al.*, 2005; ten Veldhuis and Clemens, 2011).

In fact, partial and full blockage of inlets due to the accumulation of debris is a common occurrence that can be influenced by a number of factors, including maintenance regimes, relative location of the inlet, year season (e.g. leaf fall-rate in autumn) and antecedent weather conditions (e.g. higher accumulation of tree leaves, branches and debris may occur after previous storms).

Even under correct dimensioning and positioning, large uncertainties hold about the actual operation of such simple devices due to unpredictable clogging effects, often leading to localised flooding even before the internal capacity of the drainage system is exceeded. Experimental studies addressing the clogging effect on the hydraulic efficiency of inlets are limited. The evaluation of a specific discharge law associated with a given clogging pattern is still a debated issue among researchers (Almedeij *et al.*, 2006; Guo, 2006; Gómez and Russo, 2009; Russo and Gómez, 2011; Comport and Thornton, 2012; Gómez *et al.*, 2013; Russo *et al.*, 2013; Martins *et al.*, 2014).

Because of these deficiencies, pluvial flooding events usually occur quite frequently as a consequence of rain events of lower intensity than the design one and may involve only limited portions of the urban area, even in case of proper dimensioning of the drainage system.

Given the frequent occurrence of these events, it is important to account for these circumstantial factors (inlets position, typology, clogging conditions, etc.) in urban flooding hydrodynamic models.

Therefore, hydraulic modelling of pluvial flooding in urban areas must be built upon a detailed representation of

the overland flow network of ponds and pathways to reliably represent flood propagation, also including inlets and similar devices (Despotovic *et al.*, 2005; Djordjević *et al.*, 2005). Recent availability of high-resolution digital elevation models (DEMs) has allowed flood modelling research to explore urban topography to an increased level of detail (Aronica and Lanza, 2005; Maksimović *et al.*, 2009; Fewtrell *et al.*, 2011; Gaitan *et al.*, 2012; Ozdemir *et al.*, 2013; Russo *et al.*, 2015). The assessment of the impact of surface drainage conditions and the related uncertainty on urban flooding is the general aim of the present research study. The first specific objective is the analysis of the surface drainage efficiency under various synthetic hyetographs, characterised by different construction methods and return periods. The second specific objective is to analyse the surface drainage efficiency by evaluating the combined impact of the clogging effect (relating to each inlet) and the spatial layout of inlets on pluvial flooding.

Finally, the derivation of flooding maps in a probabilistic framework is addressed.

Methods

The flood propagation model (FLURB-2D)

FLURB-2D is a two-dimensional inertial model based on the Saint Venant equations originally developed for simulating the overland flow propagation on alluvial plains with uneven topography (Aronica *et al.*, 1998) and first applied to urban areas by Aronica and Lanza (2005). Only the convective terms of the basic equations are neglected in order to eliminate the related numerical instabilities while preserving the efficiency of the hyperbolic scheme in dealing with flow fields for shallow water equations.

The original governing equations, when convective inertial terms are neglected, can be written as:

$$\begin{aligned} &\frac{\partial H}{\partial t}+\frac{\partial p}{\partial x}+\frac{\partial q}{\partial y}=0 \\ &\frac{\partial p}{\partial t}+gh\frac{\partial H}{\partial x}+ghJ_x=0 \\ &\frac{\partial q}{\partial t}+gh\frac{\partial H}{\partial y}+ghJ_y=0 \end{aligned} \tag{1}$$

where $H(t,x,y)$ is the water surface elevation; $p(t,x,y)$ and $q(t,x,y)$ are the x and y components of the unit discharge (per unit width); h is the water depth; and J_x and J_y are the hydraulic resistances in the x and y directions. If Manning's formula is adopted, these last two terms can be expressed as:

$$J_x=\frac{n^2 p\sqrt{p^2+q^2}}{h^{10/3}} \quad ; \quad J_y=\frac{n^2 q\sqrt{p^2+q^2}}{h^{10/3}} \tag{2}$$

where n is Manning's roughness factor.

The FLURB-2D model equations are solved using a Galerkin finite element technique with triangular elements (Aronica *et al.*, 1998). The water-surface elevation is assumed to be continuous and piecewise linear inside each element, where the unit discharges along the x and y directions are assumed to be constant. The finite element approach avoids a simplified description (Yu and Lane, 2006; Néelz and Pender, 2007; Chen *et al.*, 2012) of the hydraulic behaviour of flooded areas due to the fact that triangular elements are able to reproduce the detailed complex topography of the built-up areas, that is, blocks, streets and so on, exactly as they appear within the flood-prone area. In particular, blocks and other obstacles are treated as internal islands or internal boundaries within the triangular mesh covering the entire flow domain. For further details about the hydrodynamic model, the reader is referred to Aronica *et al.* (1998) and Aronica and Lanza (2005).

Although not exploited in this study, the 'physically based' description of the geometric characteristics of the calculation domain allows considering distributed rainfall hyetographs spatially varied over the domain. A modification here with respect to the model presented by Aronica and Lanza (2005) allows the inclusion of the hydraulic behaviour of the inlets in the simulation of the overland flow propagation. In the study by Aronica and Lanza (2005), inlets were considered simple sinks (outflow boundary conditions), without specifying any hydraulic characteristics of these structures.

In the new version of the model employed in this study, a typical stage discharge relationship (Brown *et al.*, 1996; Gómez *et al.*, 2011) is specified for each inlet in the following form:

$$q=c_o\cdot a\cdot h^b \tag{3}$$

where a and b are two coefficients, depending on the type (grate, curb, etc.) and geometric characteristics of the inlet (such as the number and position of the bars in the grate, gutter slope, etc.); h is the flow depth; and c_o is the efficiency coefficient. In particular, c_o represents the inlet clogging condition, thus varying between 0 and 1 (0 = total clogging, 1 = no clogging).

The hydraulic behaviour of inlets is comparable to that of a weir at low flow depths (i.e. lower than 0.12 m) and of an orifice at higher flow depths (i.e. greater than 0.12 m). The flow depth equal to 0.12 m is assumed as representative of the change in the hydraulic behaviour for the typology of inlets identified in the study area. The values of the coefficient a are assessed for each type of inlet geometry by using the following equations (after Brown *et al.*, 1996):

$$a = 0.374\mathrm{P}\sqrt{2\mathrm{g}} \quad \text{in case of weir } (h < 0.12\,\mathrm{m}) \tag{4}$$

$$a = 0.67\mathrm{A}\sqrt{2\mathrm{g}} \quad \text{in case of orifice } (h > 0.12\,\mathrm{m}) \tag{5}$$

Table 1 Coefficients of the stage discharge curve for different types of inlets

		h < 0.12 m		h > 0.12 m	
Inlet typology	Size [cm]	*a*	*b*	*a*	*b*
Grate	40 × 30	1.26	1.5	0.21	0.5
Curb	300 × 10	0.2019	1.5	0.2019	1.5
Combination	800 × 100 × 15	2.464	1.5	0.7	0.69

where P is the effective perimeter (weir length), and A is the clear opening area. The values of the exponent b are the theoretical ones for the flow depth in case of weir and orifice behaviour. Sample values of the inlet coefficients, a and b, with respect to different type of inlets and their size are provided in Table 1.

The study area

The methodological approach addressed in this study is tested on a selected study area in the town of Genoa (IT). The study area is located in the eastern part of the town centre, developed mainly during the thirties and therefore characterised by a fairly regular urban structure (grid plan). This area corresponds to the Foce neighbourhood; thus, it is named Foce subcatchment hereafter. Figure 1 provides an overview of the study area. In particular, the study area is limited on the west side by the left bank of the Bisagno Stream, completely covered in its final length (corresponding to the area of concern), while on the east side, the boundary is represented by the hill of Albaro. The northern boundary is the railway embankment, while the sea coastline determines the southern boundary. The subcatchment area is about 80 ha and is characterised by a weak slope, with a surface elevation ranging between 2.5 and 8.5 m.s.l. The area is completely urbanised, that is, streets and blocks with very limited 'pervious' parts.

The storm water drainage system is mainly separated from the sewer system, and the characteristics of the inlets operating in the Foce subcatchment, expressed in terms of typology and size, are reported in Figure 2.

The definition of the mesh was based on the morphology of the study area in order to cover the whole surface drainage network and to make internal nodes coincident with the manholes. The mesh covers only the street network of the area, and each element is considered impervious (paved or asphalted). Buildings are represented as holes in the mesh. The total meshed area is about 0.529 km^2, discretised as 56 385 triangular elements. Buildings extend for about 0.247 km^2. The geometric features (x, y, z co-ordinates) of 31 858 nodes have been derived from a DEM, with 2 m resolution obtained from an Inverse Distance Weighting interpolation operated on the digital vector map (1:5000) containing information at variable resolution (contour lines

Figure 1 Overview of the study area, the Foce subcatchment, in the town of Genoa, Italy (from Google Maps, 2015).

plus a number of measured local elevations mainly located along the streets).

The contributing area (totally paved) per inlet is a direct result of the flow hydrodynamics in the domain, and it is not necessary to define a priori which part of the catchment is connected to a single inlet. The hydrodynamic model considers only overland (pluvial) propagation, and the interactions with the subsurface drainage network are not simulated. A single value was assumed for the Manning coefficient in Eqn (2) at 0.018 s/m$^{1/3}$ over the entire domain. This value is higher than values commonly assumed for roadways and pavements made of concrete or bitumen (e.g. 0.01 s/m$^{1/3}$) and was chosen to account for the blockage effects due to the presence of debris, stones, small obstacles and so on. (Aronica and Lanza, 2005; Hunter *et al.*, 2008; Aronica *et al.*, 2012a; Schubert and Sanders, 2012).

Model boundary conditions are represented by the direct rainfall over the meshed area as inflow and the inlet stage-discharge relationship for the outflow.

Simulation scenario

The analysis is carried out by using as input synthetic hyetographs derived from the analysis of rain data collected at the rain gauge stations of Centro Funzionale (44°24′6″N; 8°56′49″E), Ponte Carrega (44°26′20″N; 8°57′48″E) and Villa Cambiaso (44°23′54″N; 8°57′47″E), located close to the study area. Rainfall data are available with fine resolution, particularly 1-min resolution for Villa Cambiaso and 5-min resolution for Centro Funzionale and Ponte Carrega

Figure 2 Location (a), type (b), geometry – in centimetres – (c) and clogging condition (d) of storm water inlets in the Foce subcatchment.

stations. The coverage of the rainfall time series for Villa Cambiaso, Ponte Carrega and Centro Funzionale is, respectively, equal to 23, 13 and 11 years.

The synthetic hyetographs are computed by using two different approaches:

- a bivariate approach based on the description of rainfall characteristics by means of copula functions (Candela *et al.*, 2014);
- a univariate approach based on the IDF curves and Chicago hyetograph (Kiefer and Chu, 1957).

A bivariate model based on the theory of copulas (Nelsen, 2006; Genest and Favre, 2007) has been used in order to analyse total rainfall volume and duration that are variables of the same phenomenon and, thus, are correlated. In the present study, the Gumbel-Hougaard one-parameter Archimedean copula has been chosen for its ability to model the dependence between physical characteristics of extreme events, for example, storm rainfall or flood hydrographs (Zhang and Singh, 2007; Requena *et al.*, 2013; Candela *et al.*, 2014; Sraj *et al.*, 2015):

$$C(u_1,u_2)=\exp\left(-\left((-\ln u)^{\theta}+(-\ln v)^{\theta}\right)^{1/\theta}\right) \tag{6}$$

with generation function:

$$\varphi(t)=[-\ln(t)]^{\theta} \quad \text{and} \quad \mathrm{t}=\mathrm{u}\,\mathrm{or}\,\mathrm{v} \tag{7}$$

where θ is the parameter of the copula function that was estimated using the method of moments with the use of the

Kendall correlation coefficient τ, and u and v are the uniformly distributed random variables $\in$ [0,1] (Nelsen, 2006; Genest and Favre, 2007).

Single annual maximum rainfall events considered here for the bivariate analysis are extracted from the series of the recorded rainfall data at the abovementioned rain gauges. An interevent time equal to 3 h was chosen here to separate the single rainfall events, for which total storm duration D, total volume storm W, average intensity $I = W/D$ and maximum intensity for specific duration were calculated.

The choice of the interevent time is usually based on considerations of the critical duration of rainfall to which the catchment responds, as stated by Acreman (1990); Heneker *et al.* (2001) and Vandenberghe *et al.* (2010). However, in order to avoid single-peak and short-duration events that could not be significant for the bivariate analysis, a larger interevent time was selected. The use of shorter interevent times has been checked, with no significant improvements.

Unlike the classical univariate approach, for multivariate analysis the definition of annual maximum event is somewhat ambiguous (Kao and Govindaraju, 2007). Extreme rainfall events could be defined as those storms that have both high volume and peak intensity.

As a matter of fact, in this study, extreme rainfall events have been defined as those storms with annual maximum joint cumulative probability of high volume and 15-min peak intensity. Moreover, as the rain gauges are located in a hydrological homogeneous area, the subsequent statistical analyses were performed by aggregating all selected events, obtaining a final sample of 45 rainfall events whose characteristics are reported in Table 2. Although records at the three sites are not mutually independent, the station-year method is applied as a long time series is not available at high resolution. However, the station-year method introduces less bias in the estimation of correlations than expected because of compensating errors (Stewart *et al.*, 1999).

Starting from the total rainfall volume–duration sample, Kendall's τ and copula parameter θ have been determined. The values obtained are 0.4537 for Kendall's τ and 1.8304 for copula parameter θ.

In order to evaluate the goodness of fit of the chosen copula, comparisons between the parametric (K_θ) and nonparametric estimate (K) of the Kendall function $K(t)$, as defined by Genest and Rivest (1993) and between isolines for empirical and theoretical copulas, are shown in Figure 3. These confirm that the Gumbel–Hougaard copula is well suited to describe the dependence structure between the available rainfall volume–duration data.

Moreover, the copula theory requires the determination of marginal distributions based on univariate data. Several extreme value distribution functions have been tested as best fitting for the total rainfall volume and duration, specifically Exponential, Gamma, Weibull, LN2 and GEV. The parameters of the marginal distributions considered were estimated by applying the maximum likelihood method, and the best fit was selected using the Akaike's Information Criterion (AIC) and the Anderson–Darling test. The results returned the log-normal probability distribution as the best marginal distribution for both total rainfall volume and duration. Figure 4 shows the two marginal distributions for the total rainfall volumes and duration compared with the empirical frequencies of the observed data.

In bivariate analysis, the choice of an appropriate joint return period (JRP) is a delicate problem. Many authors (see, e.g. Vandenberghe *et al.*, 2010; Gräaler *et al.*, 2013; Requena *et al.*, 2013; Candela *et al.*, 2014; Volpi and Fiori, 2014) stressed how different JRPs can be defined from copulas: (1) the OR return period, well known as primary return period; (2) the AND return period; and (3) the secondary return period or Kendall return period. The latter is associated with the primary return period and is defined as the mean interarrival time of events (called super-critical or dangerous events), more critical than the design event.

Although all these three return periods can be obtained using copulas thanks to their formulation, in this application, the primary return period (OR) was used because it is an intuitive extension of the definition of a univariate return period. The primary return period can be easily calculated for a bivariate copula $C(u,v)$ as:

$$T = \frac{1}{1 - C(u,v)} = \frac{1}{1 - C[P(D), P(W)]} \tag{8}$$

where $P(D)$ and $P(W)$ are the marginal distributions for total storm duration and total storm volume, respectively.

All couples (u,v) that are on the same contour (corresponding to a isoline p) of the copula C will have the same bivariate return period.

Table 2 Rainfall characteristics for the selected events at Centro Funzionale, Ponte Carrega and Villa Cambiaso (Genoa, IT)

	Event rainfall volume [mm]		Event rainfall duration [min]		15-min maximum intensity [mm/h]	
	Max	Min	Max	Min	Max	Min
Centro Funzionale	205.0	24.8	2055	175	108.0	26.4
Ponte Carrega	357.2	6.6	2060	30	203.2	21.6
Villa Cambiaso	458.0	32.8	2562	158	163.2	46.4

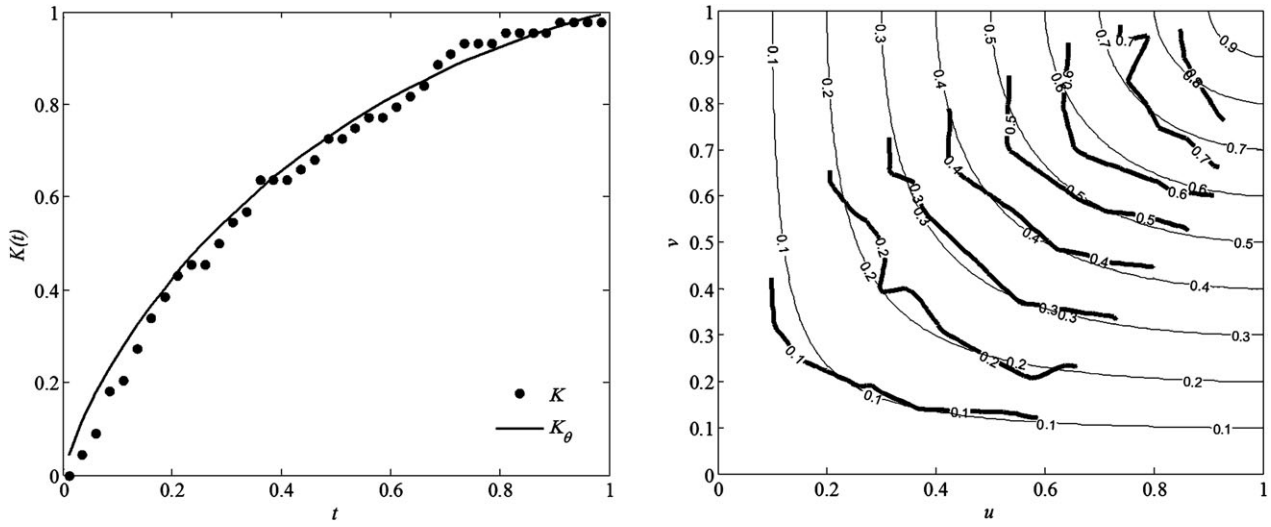

Figure 3 Comparison between the parametric (K_θ) and nonparametric (K) estimate of K(t) (left) and empirical (bold) and theoretical (light) isolines (right).

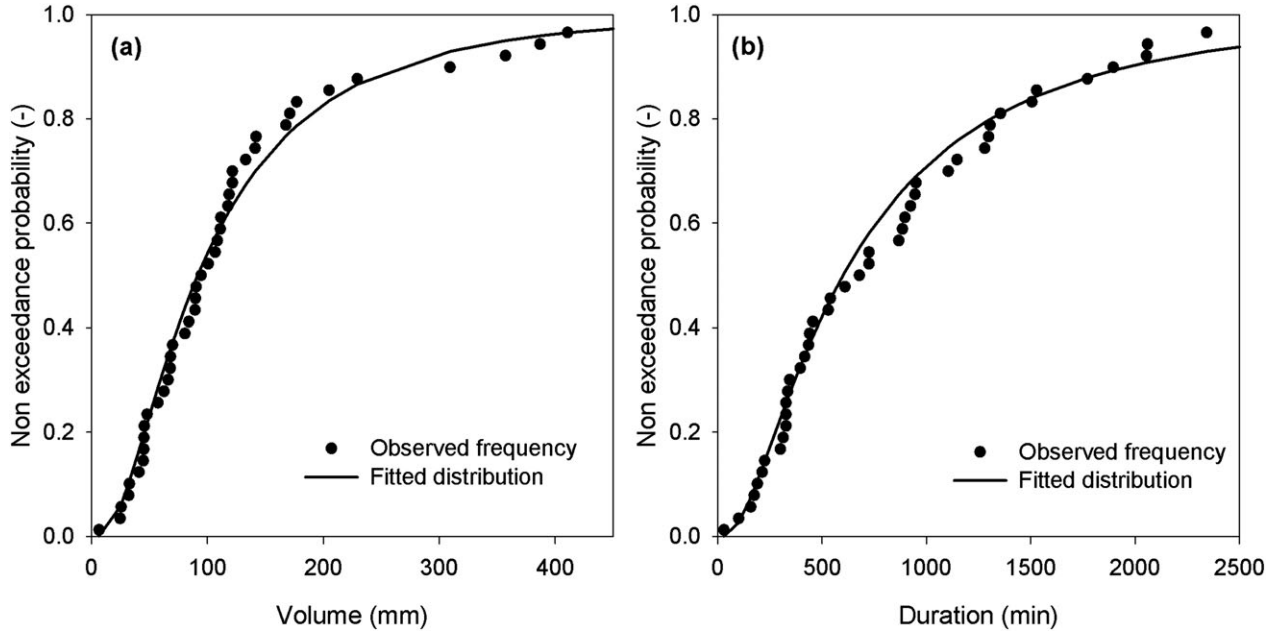

Figure 4 Plotting position: total storm volume (a) and duration (b).

Hence, for a given design return period T, the corresponding level $p = C(u,v)$ can be easily calculated using Eqn (8), and all the (D,W) pairs on the isoline p have the same return period (Figure 5).

Following Gräaler *et al.* (2013), the single design point can be selected among those lying on the isoline p as the most likely, that is, the point with the largest full bivariate density function (Figure 5, white dot).

Finally, in order to construct design storms with a realistic storm structure, the mass curve concept was considered here, as similarly implemented by various authors (Huff, 1967; Chow *et al.*, 1988; Vandenberghe *et al.*, 2010; Candela *et al.*, 2014).

To derive the mass curve for each storm, the cumulative rainfall depth at each time increment is expressed as a fraction of the total volume of the storm. Then, the time increment is also expressed as a fraction of the total duration of the storm. Figure 6 shows different mass curves constructed considering all storms using time increments equal to 1% of the storm duration. The bold black line represents the

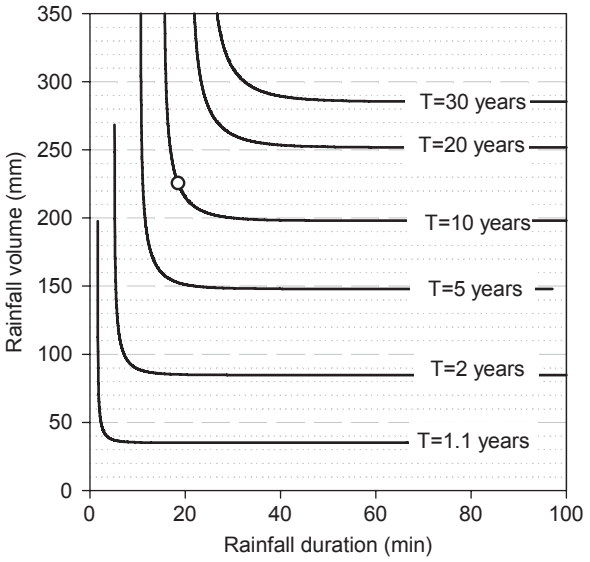

Figure 5 Joint return period values for OR for the selected copula (white dot represents the design point).

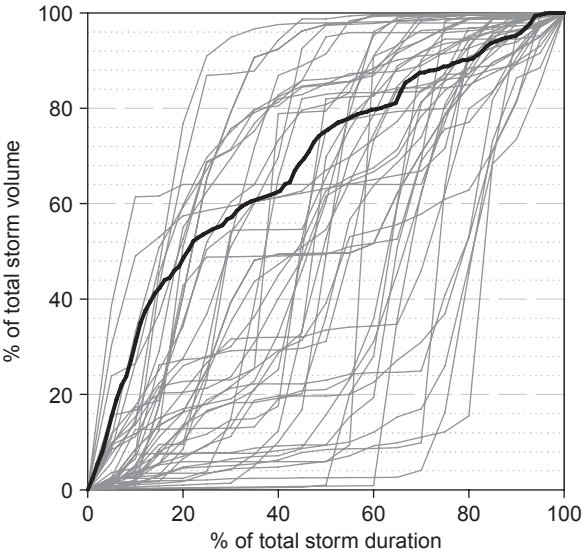

Figure 6 Mass curves for the selected storm events and generated dimensionless storm.

single-design dimensionless storm, randomly generated using a uniform sampling procedure, in the range of the 5–95% percentiles of the historical dimensionless storm.

The Chicago hyetographs are computed based on the parameters of the Villa Cambiaso Intensity–Duration–Frequency relationship for durations lower than 1 h. The rainfall duration is assumed to be equal to 60 min and the time-to-peak ratio equal to 0.5.

Figure 7 shows the Chicago hyetographs for three return periods, namely, 2, 5 and 10 years, together with the copula based hyetograph for the 10-year return period.

The two methods are here compared in order to assess the influence of the temporal distribution of rainfall events and the overall water volumes on pluvial flooding. The Chicago method has been selected in order to generate a synthetic rainfall event that shows the maximum intensity over each subevent duration; at the same time, the copula-based method has been used in order to generate more realistic total volumes.

As for the Chicago hyetographs, moving from the 2-year to the 30-year return period, the hyetograph peak (i.e. the maximum rainfall intensity over 5 min) increases from 151 to 319 mm/h, and the total rainfall depth (over the rainfall duration of 1 h) ranges from 59 to 124 mm. The event based on copula function is characterised by a maximum rainfall intensity over 5 min equal to 66 mm/h and total rainfall depth and duration, respectively, equal to 106 mm and 387 min.

In order to point out the impact of the clogging conditions of inlets on the surface drainage failures and pluvial flooding phenomena in the Foce subcatchment, a survey was carried out in October–December 2008 to investigate the actual operational conditions of the inlets. The survey was performed in the autumn season, which, for Genoa, is also the rainy season; therefore, the observed experimental data relating to the clogging conditions (opening effective area) are considered representative of the critical condition due to the falling leaves and the highest transport of solids that typically occur during the autumn and rainy season. As the plan of the maintenance operations executed by the Municipality of Genoa is unknown, the inlet cleaning regime is neglected. Based on the survey, it emerged that 5% of inlets were completely clogged, and 10% were partially clogged, generally corresponding to operational conditions where the effective area is reduced to 50% (see Figure 2). The efficiency coefficient C_0 was fixed to 0 and 0.5, respectively, for completely clogged and partially clogged inlets.

The impact of the uncertainties in the inlets' effectiveness and maintenance condition is examined here by simulating a stochastic generation of inlet efficiency scenarios by varying their clogging conditions. In particular, a Monte Carlo simulation was performed in order to generate a high number of spatially varying efficiency scenarios (1000) characterised by the overall effectiveness conditions observed during the survey (85% free, 10% partially free and 5% completely clogged).

Data analysis

The drainage efficiency of the Foce urban subcatchment is analysed by modelling the propagation of storm water exceeding the drainage capacity of the inlets in the

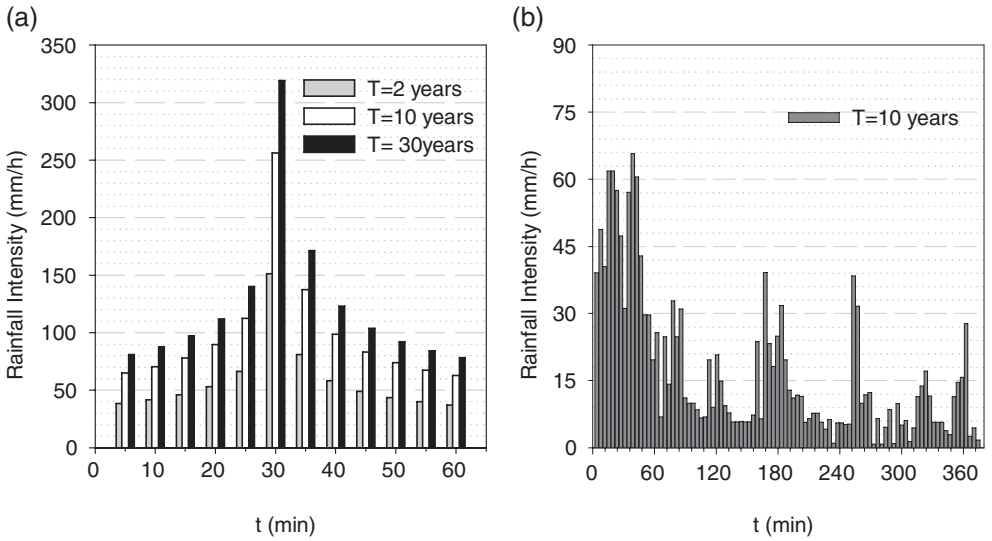

Figure 7 Chicago hyetographs for three return periods – namely 2, 10 and 30 years (a) – and copula-based hyetograph for the 10-year return period event (b).

subcatchment area. Note that simulation results are independent on the hydraulic capacity of the storm water drainage system (the pipe network); it is assumed that all water drained through any inlet node is properly conveyed to the recipient natural water body. Therefore, in the performed simulations, the occurrence of flooding is only due to drainage efficiency failures. The analysis is carried out by calculating both deterministic and probabilistic maps of the extension of pluvial flooding over the study area. Deterministic maps are obtained by plotting the maximum water depth for specific drainage efficiency scenarios. In particular, after performing a simple frequency analysis of the mean value of the maximum water depth over the entire computational domain, the scenarios corresponding to the 95th and 50th percentiles are reported and discussed.

As for the probabilistic analysis, flood occurrence probability maps and hazard class maps are computed. The flood occurrence probability maps are evaluated by converting the flooding maps into binary wet–dry maps, calculating the number of scenarios (simulations) in which a node is wet, according to a given criterion, with reference to the total number of simulations. Here, a maximum water depth greater than 0.1 m is assumed as the flooding/no flooding criterion. The hazard class maps are generated by calculating for each node the expected depth of flow, h_{flood}, as the weighted mean of the ensemble of maximum depth scenarios (Di Baldassarre *et al.*, 2009; Aronica *et al.*, 2012b). As for the weight of a given ensemble member, the Nash Sutcliff Efficiency (NSE) index (Nash and Sutcliffe, 1970), calculated with respect to the observed inlet scenario, is used. The NSE index is evaluated for each generated inlet scenario to quantitatively assess the differences between the simulated water depths in the generated and the observed scenarios. The NSE index is given by the following equation:

$$NSE = 1 - \frac{\sum_{i=1}^{n}\left(h_i - \hat{h}_i\right)^2}{\sum_{i=1}^{n}\left(h_m - \hat{h}_i\right)^2} \tag{9}$$

where h_i and $\hat{h}_i$ are the simulated water depth for the generated and the observed scenario, respectively; h_m represents the average value of the water depth for the observed scenario over the whole simulation domain; i is the node; and n is the total number of nodes. Note that NSE ranges from $-\infty$ to 1, mathematically; however, in this application, negative values of the NSE have been set to zero for consistency with the likelihood method adopted. NSE equal to one indicates a perfect match between the generated and the observed scenarios, while NSE equal to zero indicates that the generated scenario significantly differs from the observed one.

The hazard class maps are derived by considering the following hazard criteria/levels:

- $h_{\text{flood}} < 0.1$ m→hazard class = 0;
- 0.1 m < h_{flood} < 0.3 m→hazard class = 1;
- 0.3 m < h_{flood} < 0.5 m→hazard class = 2;
- $h_{\text{flood}} > 0.5$→hazard class = 3.

Results and discussion

Deterministic analysis

The maps of maximum water depth are analysed for the 10-year return period rainfall scenario. Note that the

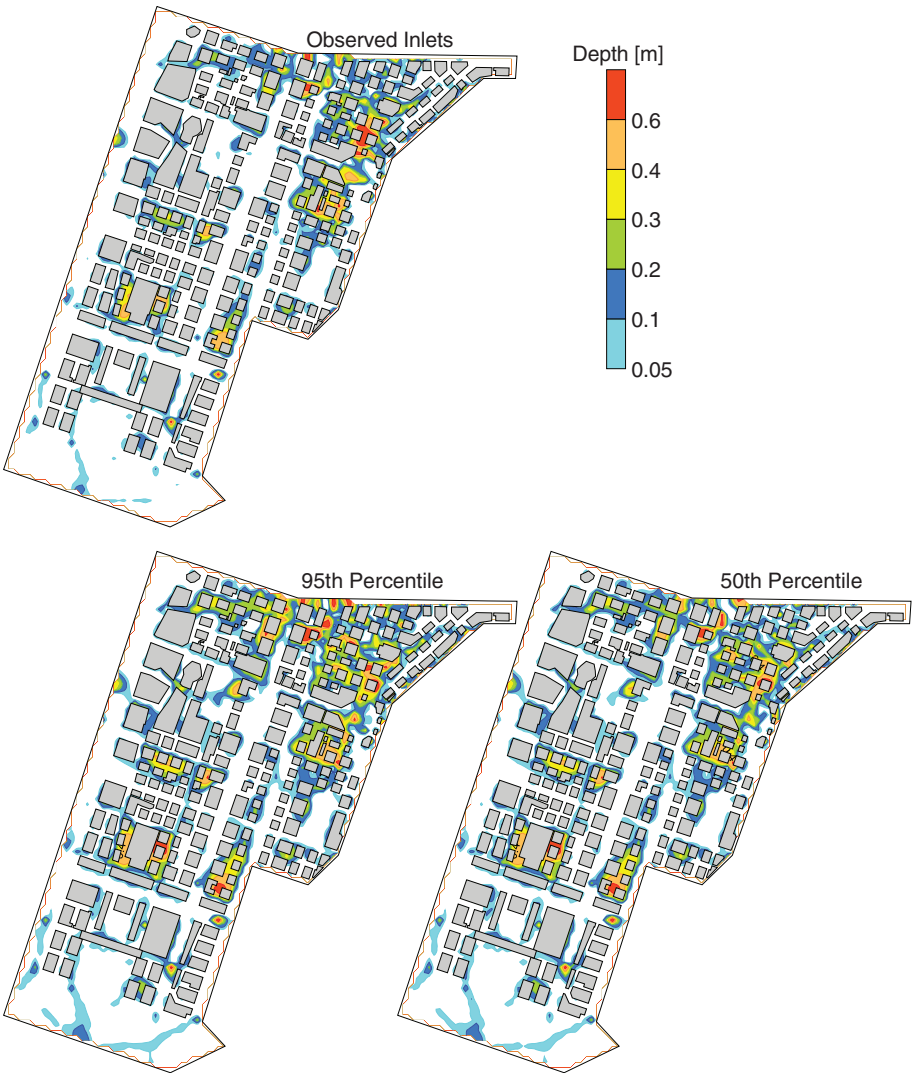

Figure 8 Maps of maximum water depth obtained for the Chicago hyetograph at the 10-year return period. The map related to the observed inlet conditions is plotted together with the maps corresponding to the 95th and 50th percentile run.

10-year return period rainfall event is a typical design event for urban drainage systems.

In Figure 8, the maps of the maximum water depth related to the observed inlet condition and to the 95th and 50th percentiles scenarios are shown for the Chicago rainfall event, with $T = 10$ years. The maps show similar flooded areas, and the dominant flow pathways are easily identified. The topographic constraints on flood inundation imply little changes in the location of flooded areas for the three inlet scenarios. By comparing the three maps, depressed areas can be highlighted in the south-central portion and in the eastern edge of the domain area. The flooded volumes increase, as expected, for the 95th percentile scenario, being itself defined in terms of mean values of the maximum water depth over the computational domain. Note that the observed condition scenario corresponds to the 85th percentile in terms of mean values of the maximum water depth.

In Figure 9, the map related to the observed inlet conditions and the 10-year copula-based hyetograph is compared with the map of the differences between the maximum water depths obtained from the Chicago and copula-based hyetographs at the 10-year return period. Concerning the observed condition scenario, the flooded volumes obtained for the copula-based hyetograph are lower than those for the Chicago hyetograph (see also Figure 8). Figure 10 illustrates the comparison between the evolution in time of the dimensionless overall water depth and cumulative rainfall for the Chicago and copula-based hyetographs. In case of the Chicago hyetograph, the maximum overall water depth is reached at the 38th min, 4 min after the rainfall hyetograph peak of

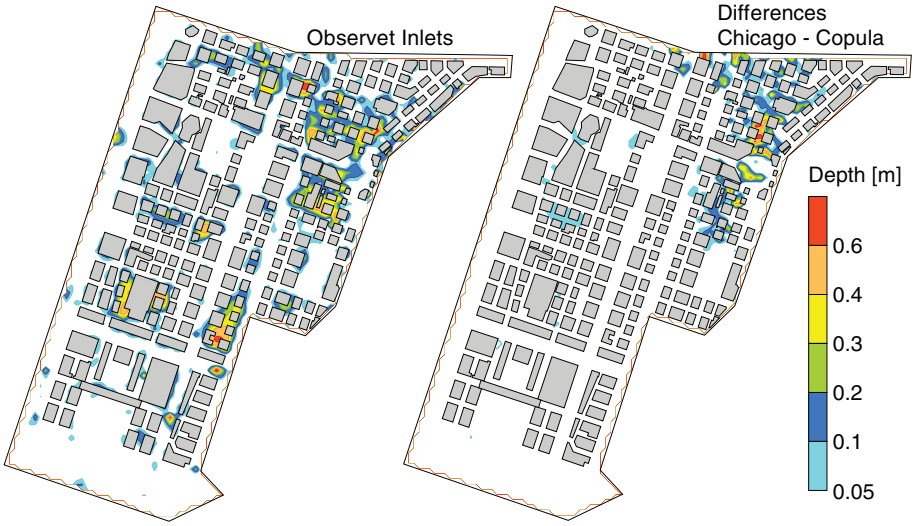

Figure 9 Maps of maximum water depth obtained for the copula-based hyetograph at the 10-year return period. The map related to the observed inlet conditions is plotted together with the map of differences between the maximum water depth obtained for the Chicago and copula-based hyetographs.

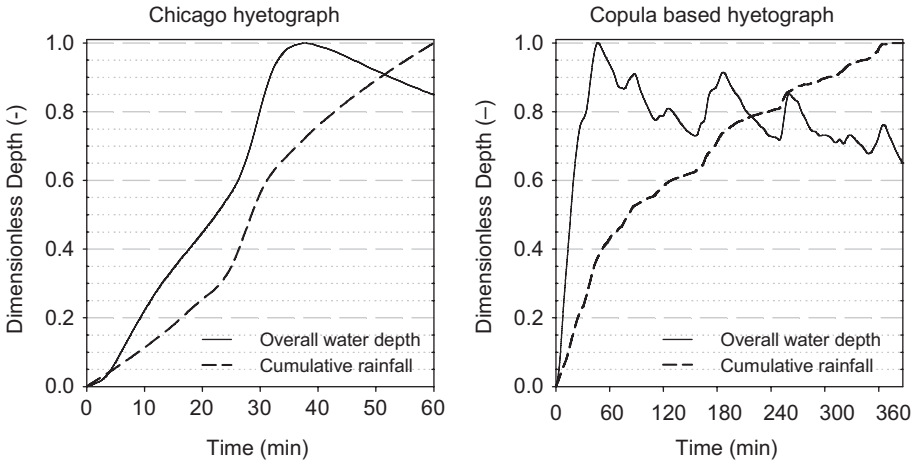

Figure 10 Comparison between the evolution in time of the dimensionless overall water depth and cumulative rainfall for the Chicago and copula-based hyetographs.

256 mm/h, while for the copula-based hyetograph, the maximum water depth is reached at the 46th min, 4 min after the rainfall hyetograph peak of 65.7 mm/h (see also Figure 7). In both cases, the overall water depth reaches the maximum value as a response to the highest rate of increase of the cumulative rainfall, that is, responding to the rainfall intensity rather than to the rainfall volume. This seems to confirm that the intensity, rather than the volume, of the forcing rainfall event drives the magnitude of pluvial flooding. The map of differences shows larger depth in the eastern edge of the domain area, while in the south-central portion, the differences are limited (i.e. lower than 0.05 m). Therefore, a lack in the surface drainage density can be detected in the eastern edge of the domain for the design storm event (T = 10 years), thus confirming the role of the inlets and inlet efficiency in storm water control.

Probabilistic analysis

Probability maps are analysed for rainfall events at 2-, 10- and 30-year return periods. The results presented in this section consider uncertainty in the inlet operational conditions and are based on an ensemble of 1000 hydrodynamic model simulations for each selected rainfall event.

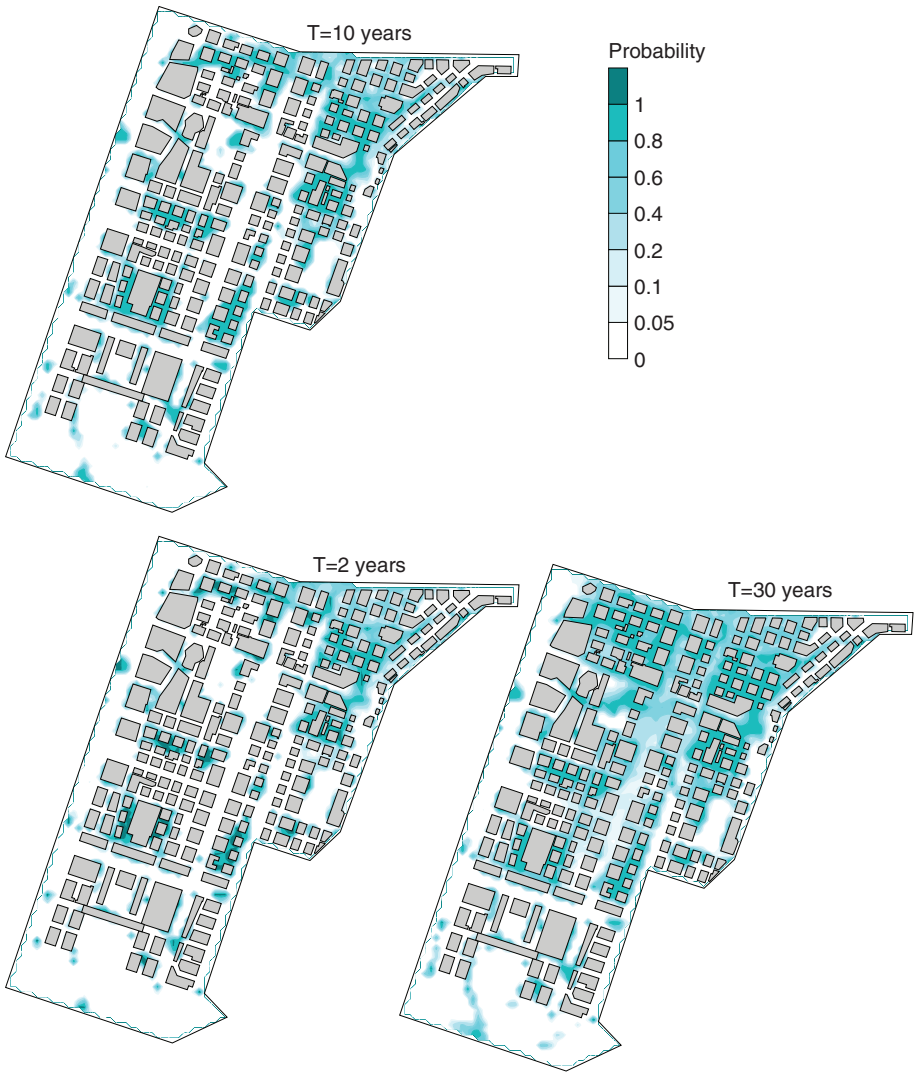

Figure 11 Flood occurrence probability maps for the Chicago hyetographs at 2-, 10- and 30-year return periods.

Figure 11 illustrates the flood occurrence probability for Chicago hyetographs at 2-, 10- and 30-year return periods. A maximum water depth greater than 0.1 m is assumed as the criterion for detecting inundation from pluvial flooding. The topographic constraints and inlet operational conditions generate little change in the flood occurrence probability over much of the domain for the 2- and 10-year return period events. A significant difference can be observed for the 30-year return period map, where the probability of flooding is high for almost the whole north-eastern portion of the domain.

In Figure , the hazard class maps are reported for Chicago hyetographs at 2-, 10- and 30-year return periods. The hazard classes are respectively characterised by h_{flood} greater than 0.1, 0.3 and 0.5 m. By comparing the three maps, the 2- and 10-year return period maps do not significantly differ, while the 30-year return period map reveals heavy flooding conditions as already observed in the flood occurrence probability map (see also Figure 11). The hazard class maps for Chicago hyetographs at the 2- and 10-year return period show localised flooded areas mainly characterised by a hazard level 1 (0.1 m < h_{flood} < 0.3 m). Inspection of both the flood occurrence probability and hazard class maps reveals that for much of the flooded domain, the water depth ranges between 0.1 and 0.3 m for events equal or greater than the design event for an urban drainage system (T = 10 years). Only in a few depressed areas, simulation depths exceed 0.3 and 0.5 m at any rainfall condition, meaning that hazard classes equal to 2 and 3 are detected for those areas, even for the 2-year return period rainfall event. As highlighted by the simulation of the Chicago hyetograph at the 30-year return period,

Figure 12 Hazard class maps for the Chicago hyetographs at 2-, 10- and 30-year return periods. The three hazard classes are respectively characterised by h_{flood} greater than 0.1, 0.3 and 0.5 m.

accumulation zones where the rainfall intensity is the major cause of water depths greater than 0.5 m (i.e. hazard class 3) can be observed in the northern portion of the domain.

Conclusions

The surface drainage efficiency of the Foce urban subcatchment in the town of Genoa (IT) has been studied by modelling the propagation of storm water on the area. In particular, the analysis has been carried out by using as input three Chicago hyetographs (T = 2, 5 and 10 years) and a bivariate copula-based hyetograph (T = 10 years). For each rainfall event, a large number of inlet efficiency scenarios are simulated. The randomness of the hydraulic efficiency of the inlets has been taken into account for a 'reliable' mapping of pluvial flooding hazard.

Simulation results allow highlighting, as expected, the occurrence of local flooded areas due to drainage failures for all precipitation events. The combined analysis of flood occurrence probability and hazard class maps confirm that topographic effects have the potential to produce local flooding with significant water depths and that local inlet operational conditions may affect the behaviour of the urban drainage system as a whole. In particular, a critical area where the specific spatial distribution of inlets enhances flooding is identified close to the eastern edge of the domain.

The results obtained for the study area confirm the suitability of the proposed methodological approach to assess the impact of the surface drainage efficiency on pluvial flooding in urban areas. The developed approach allows the

computation of flood hazard maps in a probabilistic framework, overcoming the classical problem of a single deterministic prediction of flood extent for a specific inlet configuration.

References

Acreman M.C. A simple stochastic model of hourly rainfall for Farnborough, England. *Hydrol Sci J* 1990, **35**, (2), 119–148.

Almedeij J., Alsulaili A. & Alhomoud J. Assessment of grate sag inlets in a residential area based on return period and clogging factor. *J Environ Manage* 2006, **79**, (1), 38–42.

Aronica G.T. & Lanza L.G. Drainage efficiency in the urban environment. *Hydrol Process* 2005, **19**, (5), 1105–1119.

Aronica G.T., Tucciarelli T. & Nasello C. A 2D multilevel model for flood propagation in flood affected areas. *J Water Resour Plan Manage-ASCE* 1998, **124**, (4), 210–217.

Aronica G.T., Candela A., Fabio P. & Santoro M. Estimation of flood inundation probabilities using global hazard indexes based on hydrodynamic variables. *Phys Chem Earth* 2012a, **42–44**, 119–129.

Aronica G.T., Franza F., Bates P.D. & Neal J.C. Probabilistic evaluation of flood hazard in urban areas using Monte Carlo simulation. *Hydrol Process* 2012b, **26**, (26), 3962–3972.

Ball J.E. & Alexander M. Modeling street surface runoff. In: *Proceedings of the 7th International Conference on Hydroinformatics*, Nice, France, 2006, 288–295.

Brown A.A., Stein S.M. & Warner J.C. Urban drainage design manual. HEC 22, FHWA-SA-96-078. Washington, DC: US Department of Transportation, Federal Highway Administration, 1996, 478 pp.

Candela A., Brigandì G. & Aronica G.T. Estimation of synthetic flood design hydrographs using a distributed rainfall–runoff model coupled with a copula-based single storm rainfall generator. *Nat Hazards Earth Syst Sci* 2014, **14**, (7), 1819–1833.

Chen A.S., Evans B., Djordjevic S. & Savic D.A. A coarse-grid approach to representing building blockage effects in 2D urban flood modelling. *J Hydrol* 2012, **426–427**, 1–16.

Chow V.T., Maidment D.R. & Mays L.W. *Applied hydrology*. New York, USA: McGraw-Hill International Ed, 1988.

Comport B.C. & Thornton C.I. Hydraulic efficiency of grate and curb inlets for urban storm drainage. *J Hydraul Eng* 2012, **138**, (10), 878–884.

Despotovic J., Plavsic J., Stefanovic N. & Pavlovic D. Inefficiency of storm water inlets as a source of urban floods. *Water Sci Technol* 2005, **15**, (2), 139–145.

Di Baldassarre G., Castellarin A., Montanari A. & Brath A. Probability-weighted hazard maps for comparing different flood risk management strategies: a case study. *Nat Hazards* 2009, **50**, (3), 479–496.

Djordjević S., Prodanović D., Maksimović C., Ivetić M. & Savic D. SIPSON – simulation of interaction between pipe flow and surface overland flow in networks. *Water Sci Technol* 2005, **52**, (5), 275–283.

Fewtrell T.J., Duncan A., Sampson C.C., Neal J.C. & Bates P.D. Benchmarking urban flood models of varying complexity and scale using high resolution terrestrial LiDAR data. *Phys Chem Earth* 2011, **36**, (7–8), 281–291.

Gaitan S., Veldhuis J.T., Spekkers M., & Giesen N.V.D. Urban vulnerability to pluvial flooding: complaints location on overland flow routes. In: *Proceedings of the 2nd European Conference on Flood Risk Management FLOODrisk2012*, Rotterdam, The Netherlands, 19–23 November 2012, 338–339.

Genest C. & Favre A.C. Everything you always wanted to know about copula modeling but were afraid to ask. *J Hydrol Eng-ASCE* 2007, **12**, (4), 347–368.

Genest C. & Rivest L.-P. Statistical inference procedures for bivariate Archimedean copulas. *Journal of the American Statistical Association* 1993, **88**, (423), 1034–1043.

Gómez M. & Russo B. Hydraulic efficiency of continuous transverse grates for paved areas. *J Irriga Drain Eng* 2009, **135**, (1), 225–230.

Gómez M., Macchione F. & Russo B. Methodologies to study the surface hydraulic behaviour of urban catchments during storm events. *Water Sci Technol* 2011, **63**, (11), 2666–2673.

Gómez M., Rabasseda G.H. & Russo B. Experimental campaign to determine grated inlet clogging factors in an urban catchment of Barcelona. *Urban Water J* 2013, **10**, (1), 50–61.

Gräaler B., Van den Berg M.J., Vandenberghe S., Petroselli A., Grimaldi S., De Baets B. & Verhoest N.E.C. Multivariate return periods in hydrology: a critical and practical review focusing on synthetic design hydrograph estimation. *Hydrol Earth Syst Sci* 2013, **17**, (4), 1281–1296.

Guo J.C.Y. Design of street curb opening inlets using a decay-based clogging factor. *J Hydraul Eng* 2006, **132**, 1237–1241.

Heneker T.M., Lambert M.F. & Kuczera G. A point rainfall model for risk-based design. *J Hydrol* 2001, **247**, (1–2), 54–71.

Huff F.A. Time distribution of rainfall in heavy storms. *Water Resour Res* 1967, **3**, (4), 1007–1019.

Hunter N.M., Bates P.D., Neelz S., Pender G., Villanueva I., Wright N.G. *et al.* Benchmarking 2D hydraulic models for urban flood simulations. *Proc Inst Civ Eng-Water Manage* 2008, **161**, (1), 13–30.

Kao S.C. & Govindaraju R.S. A bivariate frequency analysis of extreme rainfall with implications for design. *J Geophys Res* 2007, **112**, (13), D13119.

Kiefer C.J. & Chu H.H. Synthetic storm pattern for drainage design. *J Hydraul Div* 1957, **83**, (4), 1332/1–1332/25.

Maksimović C., Prodanović D., Boonya-Aroonnet S., Leitão J.P., Djordjević S. & Allitt R. Overland flow and pathway analysis for modelling of urban pluvial flooding. *J Hydraul Res* 2009, **47**, (4), 512–523.

Martins R., Leandro J. & de Carvalho R.F. Characterization of the hydraulic performance of a gully under drainage conditions. *Water Sci Technol* 2014, **69**, (12), 2423–2430. doi: 10.2166/wst.2014.168.

Nash J.E. & Sutcliffe J.V. River flow forecasting through conceptual models part I—a discussion of principles. *J Hydrol* 1970, **10**, (3), 282–290.

Néelz S. & Pender G. Sub-grid scale parameterisation of 2D hydrodynamic models of inundation in the urban area. *Acta Geophys* 2007, **55**, (1), 65–72.

Nelsen R.B. *An introduction to copulas*. New York: Springer-Verlag, 2006.

Ozdemir H., Sampson C.C., De Almeida G.A.M. & Bates P.D. Evaluating scale and roughness effects in urban flood modelling using terrestrial LIDAR data. *Hydrol Earth Syst Sci* 2013, **17**, (10), 4015–4030.

Requena A.I., Mediero L. & Garrote L. A bivariate return period based on copulas for hydrologic dam design: accounting for reservoir routing in risk estimation. *Hydrol Earth Syst Sci* 2013, **17**, (8), 3023–3038.

Russo B. & Gómez M. Methodology to estimate hydraulic efficiency of drain inlets. *Proc ICE-Water Manage* 2011, **164**, (2), 81–90.

Russo B., Gómez M. & Tellez J. Methodology to estimate the hydraulic efficiency of nontested continuous transverse grates. *J Irrig Drain Eng* 2013, **139**, (10), 864–871.

Russo B., Sunyer D., Velasco M. & Djordjević S. Analysis of extreme flooding events through a calibrated 1D/2D coupled model: the case of Barcelona (Spain). *J Hydroinf* 2015, **17**, (3), 473–491.

Schubert J.E. & Sanders B.F. Building treatments for urban flood inundation models and implications for predictive skill and modeling efficiency. *Adv Water Resour* 2012, **41**, 49–64.

Sraj M., Bezak N. & Brilly M. Bivariate flood frequency analysis using the copula function: a case study of the Litija station on the Sava River. *Hydrol Process* 2015, **29**, (2), 225–238.

Stewart E.J., Reed D.W., Faulkner D.S. & Reynard N.S. The FORGEX method of rainfall growth estimation, I: review of requirement. *Hydrol Earth Syst Sci* 1999, **3**, (2), 187–195.

Vandenberghe S., Verhoest N., Buyse E. & De Baets B. A stochastic design rainfall generator based on copulas and mass curves. *Hydrol Earth Syst Sci* 2010, **14**, (12), 2429–2442.

ten Veldhuis J.A.E. & Clemens F.H.L.R. The efficiency of asset management strategies to reduce urban flood risk. *Water Sci Technol* 2011, **64**, (6), 1317–1324.

Volpi E. & Fiori A. Hydraulic structures subject to bivariate hydrological loads: return period, design, and risk assessment. *Water Resour Res* 2014, **50**, (2), 885–897.

Yu D. & Lane S.N. Urban fluvial flood modelling using a two-dimensional diffusion-wave treatment, part 1: mesh resolution effects. *Hydrol Process* 2006, **20**, (7), 1541–1565.

Zhang L. & Singh V.P. Bivariate rainfall frequency distributions using Archimedean copulas. *J Hydrol* 2007, **332**, (1–2), 93–109.

